

Scaling in many-body systems and proton response

Omar Benhar

INFN, Sezione Roma 1

Dipartimento di Fisica, Università “La Sapienza”

Piazzale Aldo Moro, 2. I-00185 Roma, Italy

(November 8, 2018)

Abstract

The observation of scaling in processes in which a weakly interacting probe delivers large momentum \mathbf{q} to a many-body system reflects the dominance of incoherent scattering off target constituents. While a suitably defined scaling function can provide rich information on the internal dynamics of the target, in general its extraction from the measured cross section requires careful consideration of the nature of the interaction driving the scattering process. The analysis of deep inelastic electron-proton scattering in the target rest frame within standard many-body theory naturally leads to the emergence of a scaling function that, unlike the commonly used structure functions F_1 and F_2 , can be identified with the intrinsic proton response. The implications for the theoretical analysis of deep inelastic scattering and the interpretation of the data are discussed.

PACS numbers: 13.60.Hb,24.10.Cn,61.12.Bt

Typeset using REVTeX

I. INTRODUCTION

Scaling is observed in a variety of scattering processes involving many-body systems [1]. For example, at large momentum transfer $|\mathbf{q}|$ the response of liquid helium measured by inclusive scattering of thermal neutrons, which in general depends upon *both* \mathbf{q} and the energy transfer ν , exhibits a striking scaling behavior, i.e. it becomes a function of the single variable $y = (m/|\mathbf{q}|)(\nu - \mathbf{q}^2/2m)$, m being the mass of the helium atom [2]. Scaling in a similar variable occurs in inclusive electron-nucleus scattering at $|\mathbf{q}| > 500$ MeV and electron energy loss $\nu < Q^2/2M$, where $Q^2 = |\mathbf{q}|^2 - \nu^2$ and M is the nucleon mass [3]. Another most celebrated example is scaling of the deep inelastic proton structure functions, measured by lepton scattering at large Q^2 , in the Bjorken variable $x = Q^2/2M\nu$ [4].

The relation between Bjorken scaling and scaling in the variable y , whose definition and interpretation emerge in a most natural fashion from the treatment of the scattering process in the target rest frame within many-body theory, has been discussed by many authors (see, e.g., ref. [5]). Recently, deep inelastic data have been also shown to scale in the variable $\tilde{y} = \nu - |\mathbf{q}|$ [6], related to *both* y and the Nachtmann variable ξ [7], which in turn coincides with x in the $Q^2 \rightarrow \infty$ limit.

The observation of scaling in processes driven by different interactions clearly indicates that its occurrence reflects the dominance of a common reaction mechanism, independent of the underlying dynamics. In all instances, scaling is indeed a consequence of the onset of the kinematical regime in which scattering of a weakly interacting probe by a composite target reduces to the incoherent sum of elementary scattering processes involving its constituents.

While the primary goal of scaling analysis is the identification of the dominant reaction mechanism, it has to be also emphasized that the scaling variable has a straightforward physical interpretation, and a suitably defined scaling function, being directly related to the target response, contains a great deal of dynamical information.

In general, extracting the target response from the measured cross section requires careful consideration of the nature of the interaction driving the scattering process. In neutron-

liquid helium scattering, due to the scalar character of the probe-constituent coupling, the cross section coincides with the response up to a kinematical factor [2]. On the other hand, in electromagnetic processes the internal dynamics of the target and the probe-constituent interaction are nontrivially coupled. As a consequence, to obtain the target response in the case of electron-nucleus scattering one has to devise a procedure to remove from the data the dependence upon the elementary electron-nucleon cross section [3]. In this paper I will discuss the extension of this method to the analysis of deep inelastic scattering (DIS) of electrons by protons.

The theoretical treatment of scattering off a many-body system and the emergence of scaling as a consequence of the assumptions involved in the impulse approximation (IA) are outlined in Section II, where the case of neutron-liquid helium scattering is considered as a pedagogical example. The procedure leading to identify the target response and the scaling variable in the more complex case of electron-nucleus scattering is traced in Section III, while Section IV describes the application of the same procedure to deep inelastic electron-proton scattering, and compares the resulting analysis to the standard Bjorken scaling analysis. The implications of the proposed approach for both the theoretical description of DIS and the interpretation of the data are discussed in Section V. Finally, Section VI summarizes the main results and states the conclusions.

II. SCATTERING OFF MANY-BODY SYSTEMS IN THE IA REGIME AND *y*-SCALING

A. Target response function

Let us consider scattering off a nonrelativistic bound system consisting of N *pointlike* particles of mass m , and assume that the probe-target interaction be *scalar* and *weak*, so that Born approximation can safely be used. The differential cross section of the process in which a beam particle, carrying momentum \mathbf{k} and energy E , is scattered into the solid

angle $d\Omega$ with energy $E' = E - \nu$ and momentum \mathbf{k}' can be written

$$\frac{d\sigma}{d\Omega dE'} = \frac{\sigma}{4\pi} \frac{|\mathbf{k}'|}{|\mathbf{k}|} S(\mathbf{q}, \nu), \quad (1)$$

where σ is the probe-constituent total cross section. The *response function* $S(\mathbf{q}, \nu)$, containing all the information on the structure of the target, is defined as

$$S(\mathbf{q}, \nu) = \sum_n |\langle n | \rho_{\mathbf{q}} | 0 \rangle|^2 \delta(\nu + E_0 - E_n) \quad (2)$$

$$= \int \frac{dt}{2\pi} e^{i\nu t} \langle 0 | \rho_{\mathbf{q}}^\dagger(t) \rho_{\mathbf{q}}(0) | 0 \rangle, \quad (3)$$

where

$$\rho_{\mathbf{q}}(t) = e^{iHt} \rho_{\mathbf{q}} e^{-iHt}, \quad (4)$$

H is the hamiltonian describing the internal dynamics of the target and

$$\rho_{\mathbf{q}} = \sum_{\mathbf{p}} a_{\mathbf{p}+\mathbf{q}}^\dagger a_{\mathbf{p}}, \quad (5)$$

$a_{\mathbf{p}}^\dagger$ and $a_{\mathbf{p}}$ being constituent creation and annihilation operators, respectively. The target ground and final states $|0\rangle$ and $|n\rangle$ satisfy the many-body Schrödinger equations $H|0\rangle = E_0|0\rangle$ and $H|n\rangle = E_n|n\rangle$.

Rewriting Eq.(2) in coordinate space we obtain

$$S(\mathbf{q}, \nu) = \sum_n \left| \int dR \langle n | R \rangle \sum_{i=1}^N e^{i\mathbf{q}\cdot\mathbf{r}_i} \langle R | 0 \rangle \right|^2 \delta(\nu + E_0 + E_n), \quad (6)$$

where $R \equiv (\mathbf{r}_1, \dots, \mathbf{r}_N)$ specifies the target configuration, $\langle R | 0 \rangle$ and $\langle R | n \rangle$ denote the target initial and final state wave functions, respectively, and the index i labels the struck constituent.

The main assumption underlying IA is that, as the space resolution of a probe delivering momentum \mathbf{q} is $\sim 1/|\mathbf{q}|$, at large enough $|\mathbf{q}|$ (typically $|\mathbf{q}| \gg 2\pi/d$, d being the average separation between target constituents) the target is seen by the probe as a collection of individual particles. In addition, final state interactions (FSI) between the hit constituent,

carrying large momentum $\sim \mathbf{q}$, and the residual $(N - 1)$ -particle system are assumed to be negligibly small.

In the IA regime the scattering process reduces to the incoherent sum of elementary processes involving only one constituent, the remaining $(N - 1)$ particles acting as spectators, and Eq.(6) takes the simple form

$$S(\mathbf{q}, \nu) = \sum_i \sum_n \left| \int dR \langle n|R \rangle e^{i\mathbf{q}\cdot\mathbf{r}_i} \langle R|0 \rangle \right|^2 \delta(\nu + E_0 + E_n) . \quad (7)$$

On account of the absence of FSI, the IA final state $|n\rangle$, carrying total momentum \mathbf{q} , exhibits the product structure

$$|n\rangle = |\mathbf{p}', \mathcal{R}\rangle = |\mathbf{p}'\rangle \otimes |\mathcal{R}(\mathbf{q} - \mathbf{p}')\rangle , \quad (8)$$

its energy being given by

$$E_n = E_{\mathbf{p}'} + E_{\mathcal{R}} . \quad (9)$$

In the above equations $|\mathbf{p}'\rangle$ denotes the state describing a free particle carrying momentum \mathbf{p}' and energy $E_{\mathbf{p}'} = |\mathbf{p}'|^2/2m$, while $E_{\mathcal{R}}$ is the energy of the the spectator $(N - 1)$ -particle system, left in the state $|\mathcal{R}\rangle$ with momentum $\mathbf{q} - \mathbf{p}'$. As a consequence, the sum over final states appearing in Eq.(6) can be carried out replacing

$$\sum_n |n\rangle\langle n| \rightarrow \int d^3p' |\mathbf{p}'\rangle\langle\mathbf{p}'| \sum_{\mathcal{R}} |\mathcal{R}(\mathbf{q} - \mathbf{p}')\rangle\langle\mathcal{R}(\mathbf{q} - \mathbf{p}')| . \quad (10)$$

Substitution of Eqs.(8)-(10) into Eq.(7) leads to (see, e.g., ref. [8])

$$S(\mathbf{q}, \nu) = \int d^3p \int d\epsilon P(\mathbf{p}, \epsilon) \delta(\nu + \epsilon - E_{\mathbf{p}+\mathbf{q}}) , \quad (11)$$

where the function

$$P(\mathbf{p}, \epsilon) = \sum_{\mathcal{R}} |\langle 0|\mathbf{p}, \mathcal{R}\rangle|^2 \delta(\epsilon + E_{\mathcal{R}} - E_0) \quad (12)$$

gives the probability of finding a target constituent with momentum \mathbf{p} and energy ϵ in the target ground state.

B. y -scaling: neutron scattering off liquid helium as an example

Eqs.(11) and (12) show that the IA response only depends upon \mathbf{q} and ν through the energy-conserving δ -function, requiring

$$\nu + E_0 - E_{\mathcal{R}} - E_{\mathbf{p}+\mathbf{q}} = 0 . \quad (13)$$

The occurrence of scaling, i.e. the fact that, up to a kinematical factor $K(|\mathbf{q}|, \nu)$, $S(\mathbf{q}, \nu)$ becomes a function of a single variable, simply reflects the fact that in the IA regime, in which energy conservation is expressed by Eq.(13), \mathbf{q} and ν are no longer independent variables. One can then define a new variable $y = y(\mathbf{q}, \nu)$ such that, as $|\mathbf{q}| \rightarrow \infty$,

$$K(|\mathbf{q}|, \nu)S(\mathbf{q}, \nu) \rightarrow F(y) . \quad (14)$$

All the above results can be immediately applied to the case of neutron scattering off liquid helium, in which the energy dependence of $P(\mathbf{p}, \epsilon)$ can be safely neglected and Eq.(13) takes the form [8]

$$\nu + \frac{\mathbf{p}^2}{2m} - \frac{|\mathbf{p} + \mathbf{q}|^2}{2m} = 0 , \quad (15)$$

m being the mass of the helium atom. It follows that, defining

$$y = \frac{m}{|\mathbf{q}|} \left(\nu - \frac{|\mathbf{q}|^2}{2m} \right) , \quad (16)$$

one can rewrite the response in the form

$$S(\mathbf{q}, \nu) = \frac{m}{|\mathbf{q}|} 2\pi \int_{|y|}^{\infty} |\mathbf{p}| d|\mathbf{p}| n(|\mathbf{p}|) , \quad (17)$$

with the constituent momentum distribution defined as

$$n(|\mathbf{p}|) = \int d\epsilon P(\mathbf{p}, \epsilon) . \quad (18)$$

Eq.(17) implies that in the $|\mathbf{q}| \rightarrow \infty$ limit

$$\frac{|\mathbf{q}|}{m} S(\mathbf{q}, \nu) \rightarrow F(y) , \quad (19)$$

the kinematical factor being given by $K(|\mathbf{q}|, \nu) = |\partial\nu/\partial p_{\parallel}| = |\mathbf{q}|/m$, with $p_{\parallel} = \mathbf{p} \cdot \mathbf{q}/|\mathbf{q}|$.

Fig.1 displays the behavior of $F(y)$, defined by the above equation, measured in neutron scattering off superfluid ^4He at $T = 1.6 \text{ }^\circ\text{K}$ [9]. It clearly appears that the curves corresponding to $|\mathbf{q}| > 15 \text{ \AA}^{-1}$ lie on top of one another, indicating the onset of the scaling regime.

The variable y defined by Eq.(16) does have a straightforward physical interpretation, as does the scaling function of Eq.(19). The scaling variable can be identified with the initial longitudinal momentum of the struck atom, p_{\parallel} , while $F(y)$ can be related to the momentum distribution through

$$n(|\mathbf{p}|) = -\frac{1}{2\pi} \frac{1}{|\mathbf{p}|} \left(\frac{dF}{dy} \right)_{|y|=|\mathbf{p}|} . \quad (20)$$

The relation linking the response in the scaling regime to $n(|\mathbf{p}|)$ has been extensively exploited to extract momentum distributions of normal and superfluid ^4He from neutron scattering data [10].

III. SCALING IN ELECTRON SCATTERING

A. Scattering cross section in the IA regime

The unpolarized electron scattering cross section is usually written in the form (see, e.g., ref. [11])

$$\frac{d^2\sigma}{d\Omega dE'} = \frac{\alpha^2}{Q^4} \frac{E'}{E} L_{\mu\nu} W^{\mu\nu} , \quad (21)$$

where E and E' denote the initial and final electron energy, respectively, $Q^2 = -q^2$, $q = k - k' \equiv (\nu, \mathbf{q})$ being the four-momentum transfer, and α is the fine structure constant. The electron tensor $L_{\mu\nu}$ is fully specified by the measured kinematical variables. In the limit of ultrarelativistic electrons it reads

$$L_{\mu\nu} = 2 \left[k_{\mu} k'_{\nu} + k_{\nu} k'_{\mu} - g^{\mu\nu} (kk') \right] . \quad (22)$$

The information on the structure of the target is contained in the tensor $W_{\mu\nu}$, which can be written in a form reminiscent of Eqs.(2) and (3) replacing the density fluctuation operator $\rho_{\mathbf{q}}$ with the electromagnetic current J^μ . The resulting expression reads

$$W^{\mu\nu} = \sum_n \langle 0|J^{\mu\dagger}|n\rangle \langle n|J^\nu|0\rangle \delta^{(4)}(P_0 + q - P_n) \quad (23)$$

$$= \int \frac{d^4x}{(2\pi)^4} e^{iqx} \langle 0|J^{\mu\dagger}(x)J^\nu(0)|0\rangle, \quad (24)$$

where $P_0 \equiv (M, \mathbf{0})$, M being the target mass, and P_n denote the four-momenta of the target initial and final states, respectively.

In the IA scheme the target tensor of Eqs.(23) and (24) is replaced by a weighted sum of tensors describing the electromagnetic structure of target constituents (compare to Eq.(11)):

$$W^{\mu\nu} \rightarrow \sum_i \int d^4p P(p) w_i^{\mu\nu}(\tilde{p}, \tilde{q}) \delta(\nu + p_0 - E_{\mathbf{p}+\mathbf{q}}), \quad (25)$$

where $E_{\mathbf{p}+\mathbf{q}} = \sqrt{|\mathbf{p} + \mathbf{q}|^2 + m^2}$, m being the constituent mass, $\tilde{p} \equiv (E_{\mathbf{p}}, \mathbf{p})$, with $E_{\mathbf{p}} = \sqrt{|\mathbf{p}|^2 + m^2}$, and $\tilde{q} \equiv (\tilde{\nu}, \mathbf{q})$, with $\tilde{\nu} = E_{\mathbf{p}+\mathbf{q}} - E_{\mathbf{p}} = \nu + p_0 - E_{\mathbf{p}}$. The distribution function $P(p)$ yields the probability to find a constituent carrying four-momentum $p \equiv (p_0, \mathbf{p})$ in the target ground state. It has to be emphasized that the tensor $w_i^{\mu\nu}$ describes the electromagnetic interaction of the i -th target constituent in free space. Hence, the above equation shows that the IA formalism allows one to describe scattering off a *bound* constituent in terms of the electromagnetic tensor associated with a *free* constituent, binding effects being taken care of by replacing p, q with \tilde{p}, \tilde{q} (see Appendix A).

Note that, on account of the replacement $q \rightarrow \tilde{q}$, $w_i^{\mu\nu}$ is manifestly *non* gauge-invariant, as $q_\mu w^{\mu\nu} \neq 0$. A somewhat *ad hoc* prescription to restore gauge invariance, widely used in the theoretical analysis of electron-nucleus scattering data, has been proposed by De Forest back in the 80s [12] (see Appendix B). More recently, the problem of reconciling IA and current conservation in DIS has been discussed in ref. [13]. It has to be emphasized that, although in general violation of gauge invariance is an unpleasant feature inherent in the IA scheme, it does not play a role in the $|\mathbf{q}| \rightarrow \infty$ limit, in which the non gauge-invariant contributions to the current can be shown to be vanishingly small.

Substitution of the IA target tensor (25) into Eq.(21) yields

$$\frac{d\sigma}{d\Omega dE'} = \sum_i \int d^4p P(p) \left(\frac{d\sigma_i}{d\Omega dE'} \right) \delta(\nu + p_0 - E_{\mathbf{p}+\mathbf{q}}) , \quad (26)$$

where $(d\sigma_i/d\Omega dE')$ is the elementary electron-constituent cross section, whose structure will be discussed in the next Section.

B. Extracting the target response from the cross section

From Eqs.(21), (25) and (26) it follows that

$$\left(\frac{d\sigma_i}{d\Omega dE'} \right) = \frac{\alpha^2}{Q^4} \frac{E'}{E} L_{\mu\nu} \tilde{w}_i^{\mu\nu} = \left(\frac{d\sigma}{d\Omega} \right)_M \left[\sigma_{i_2} + 2 \sigma_{i_1} \tan^2 \frac{\theta}{2} \right] , \quad (27)$$

where $(d\sigma/d\Omega)_M$ denotes the Mott cross section, θ is the electron scattering angle and $\tilde{w}_i^{\mu\nu}$ is the electromagnetic tensor associated with the i -th constituent, corrected to restore gauge invariance, whose definition is given in Appendix B. The functions σ_{i_1} and σ_{i_2} can be written

$$\sigma_{i_1} = \frac{m^2}{E_{\mathbf{p}} E_{\mathbf{p}+\mathbf{q}}} \left(w_{i_1} + \frac{1}{2} \frac{p_{\perp}^2}{m^2} w_{i_2} \right) \quad (28)$$

and

$$\sigma_{i_2} = \frac{m^2}{E_{\mathbf{p}} E_{\mathbf{p}+\mathbf{q}}} \frac{q^2}{|\mathbf{q}|^2} \left\{ w_{i_1} \left(\frac{\tilde{q}^2}{q^2} - 1 \right) + \frac{w_{i_2}}{m^2} \left[\frac{q^2}{|\mathbf{q}|^2} \left(E_p - \tilde{\nu} \frac{(\tilde{q}\tilde{p})}{\tilde{q}^2} \right)^2 - \frac{p_{\perp}^2}{2} \right] \right\} , \quad (29)$$

where p_{\perp} is the component of the constituent momentum perpendicular to the momentum transfer and w_{i_1} and w_{i_2} are the *constituent structure functions*.

Substitution of Eqs.(27)-(29) into Eq.(26) finally leads to the familiar expression of the electron scattering cross section in terms of the two *target structure functions* W_1 and W_2 :

$$\frac{d^2\sigma}{d\Omega dE'} = \left(\frac{d\sigma}{d\Omega} \right)_M \left[W_2 + 2W_1 \tan^2 \frac{\theta}{2} \right] , \quad (30)$$

with

$$W_{1,2} = \sum_i \int d^4p P(p) \sigma_{i_{1,2}}(p, q) \delta \left(\nu + p_0 - \sqrt{|\mathbf{p} + \mathbf{q}|^2 + m^2} \right) . \quad (31)$$

Eq.(26) shows that in the case of electron scattering the target structure function does not appear as a multiplicative factor in the cross section. In principle, the p -dependence of the elementary cross section, coupling the internal dynamics of the target to the probe-constituent interaction, prevents one from extracting the structure function from the data. In addition, as the integrand in the right hand side of Eqs.(26) depends upon q through *both* ($d\sigma_i/d\Omega dE'$) *and* the argument of the energy conserving δ -function, the occurrence of y -scaling can no longer be established using the simple argument of Section II.

The above problems can be circumvented exploiting the weak momentum and energy dependence of the elementary cross section. Assuming that the distribution function $P(p)$ be a rapidly decreasing function, the elementary cross section can be evaluated at a constant $p = \bar{p}$, corresponding to the peak of $P(p)$, and moved out of the integral. As a result, one can readily identify the target response with the ratio

$$S(\mathbf{q}, \nu) = \frac{d\sigma}{d\Omega dE'} \bigg/ \sum_i \left(\frac{d\sigma_i}{d\Omega dE'} \right)_{p=\bar{p}} . \quad (32)$$

Note that, as $S(\mathbf{q}, \nu)$ defined by the above equation depends upon q only through the energy conserving delta function, it is also expected to exhibit y -scaling.

C. y -scaling in electron-nucleus scattering

The procedure described in the previous Section has been extensively employed to analyze electron-nucleus (eA) scattering data. Although in this case the target constituents (Z protons and $N = A - Z$ neutrons) are not structureless, y -scaling still occurs as long as the internal degrees of freedom of the constituents are not excited by the interaction with the electron probe, i.e. as long as the elementary electron-nucleon scattering process is elastic. In this case, the nucleon structure functions entering Eqs.(28) and (29) can be written ($i = p, n$)

$$w_{i_1} = -\frac{\tilde{q}^2}{4m^2} (F_{i_1} + \kappa F_{i_2})^2 \quad (33)$$

and

$$w_{i_2} = \left[F_{i_1}^2 - \frac{\tilde{q}^2}{4m^2} (\kappa_i F_{i_2})^2 \right], \quad (34)$$

where F_{i_1} and F_{i_2} are the Dirac and Pauli form factors, respectively, and κ_i denotes the nucleon anomalous magnetic moment.

In analogy with the case of neutron scattering off liquid helium, the requirement of energy conservation provides the definition of the scaling variable through

$$\nu + M - \sqrt{(y + |\mathbf{q}|)^2 + m^2} - \sqrt{y^2 + (M - m + B_0)^2} = 0, \quad (35)$$

where B_0 is the (positive) minimum nucleon binding energy. The corresponding scaling function is

$$F(y) = K(\mathbf{q}, y) \frac{1}{(Z\bar{\sigma}_p + N\bar{\sigma}_n)} \left(\frac{d\sigma}{d\Omega dE'} \right) \quad (36)$$

where $K(\mathbf{q}, y) = |\partial\nu/\partial p_{\parallel}|_{p=\bar{p}}$.

Fig.2 shows the cross sections recently measured at the Thomas Jefferson National Accelerator Facility scattering 4 GeV electrons off an Iron target [14]. The corresponding scaling functions, obtained from the definitions of Eqs.(35) and (36), are shown in fig.3. It clearly appears that the data, covering the range of momentum transfer $1 < |\mathbf{q}| < 4$ GeV, exhibit a striking scaling behaviour at $y < 0$. The scaling violations observed in the region of positive y , corresponding to large electron energy loss, have to be ascribed to the occurrence of inelastic electron-nucleon scattering.

Although the scaling variable defined by Eq.(35) can still be related to the longitudinal momentum of the struck nucleon, in the case of eA scattering the constituent binding energy plays a significant role, making it more difficult to establish a direct relation between $F(y)$ and the nucleon momentum distribution $n(|\mathbf{p}|)$. A procedure to extract $n(|\mathbf{p}|)$ from eA data in the y -scaling regime taking into account binding corrections has been developed in ref. [15].

IV. SCALING IN DEEP INELASTIC SCATTERING AND PROTON RESPONSE

A. The proton as a many-body system

Let us now make the rather strong assumption that the proton can be viewed as a many-body system consisting of *bound* pointlike Dirac particles of mass m and charge e_i (in units of the magnitude of the electron charge), and extend the analysis described in the previous Sections to deep inelastic electron-proton (ep) scattering. In this scenario, as in the standard parton model of DIS [11], one assumes that over the short spacetime scale relevant to the scattering process confinement does not play a role, so that proton constituents can be described in terms of physical states. It has to be emphasized, however, that, unlike the parton model, the present approach *does not* involve the additional assumption that proton constituents be on mass shell.

The structure functions appropriate for the case of pointlike constituents are (compare to Eqs.(33) and (34))

$$w_{i_1} = -e_i^2 \frac{\tilde{q}^2}{4m^2} \quad (37)$$

and

$$w_{i_2} = e_i^2 . \quad (38)$$

The requirement of energy conservation, expressed by the equation

$$\nu + p_0 - \sqrt{|\mathbf{p} + \mathbf{q}|^2 + m^2} = \nu + p_0 - p_{\parallel} - |\mathbf{q}| + \mathcal{O}\left(\frac{1}{|\mathbf{q}|}\right) = 0 , \quad (39)$$

where $p_0 = M - E_{\mathcal{R}}$ and $E_{\mathcal{R}} = \sqrt{|\mathbf{p}|^2 + M_{\mathcal{R}}^2}$, $M_{\mathcal{R}}$ being the mass of the spectator system, implies that, as $|\mathbf{q}| \rightarrow \infty$, the quantity

$$\tilde{y} = \nu - |\mathbf{q}| = p_{\parallel} - p_0 \quad (40)$$

becomes independent of \mathbf{q} . Hence, in this limit $S(\mathbf{q}, \nu)$, defined as in eq.(32), is expected to exhibit scaling in the variable \tilde{y} [6], i.e.

$$S(\mathbf{q}, \nu) \rightarrow F(\tilde{y}). \quad (41)$$

Note that in this case the kinematical factor entering the definition of the scaling function is $|\partial\nu/\partial p_{\parallel}| \equiv 1$.

It has to be pointed out that \tilde{y} *does not* have the same physical interpretation as the variable y discussed in the previous sections: it *does not* coincide with the constituent longitudinal momentum. However, as p_0 is independent of q , scaling in $y = p_{\parallel}$ necessarily implies scaling in \tilde{y} , and *viceversa*. The motivation for choosing \tilde{y} as scaling variable in DIS will be discussed in the next Section.

B. \tilde{y} -scaling analysis of DIS data

According to the IA picture, the \tilde{y} -scaling function can be obtained dividing either structure function by the appropriate contribution to the elementary cross section. In fact, from Eqs.(30)-(32) and (41) it follows that, in the $|\mathbf{q}| \rightarrow \infty$ limit,

$$S(\mathbf{q}, \nu) = \frac{W_1}{\bar{\sigma}_1} = \frac{W_2}{\bar{\sigma}_2} \rightarrow F(\tilde{y}) , \quad (42)$$

where

$$\bar{\sigma}_{1,2} = \sum_i (\bar{\sigma}_{i,2})_{p=\bar{p}} , \quad (43)$$

with $\bar{p} \equiv (\bar{p}_0, \mathbf{p}_{min})$, \mathbf{p}_{min} being the minimum constituent momentum allowed in the kinematics specified by \mathbf{q} and ν . The magnitude of \mathbf{p}_{min} is given by

$$|\mathbf{p}_{min}| = \frac{1}{2} \left| \frac{M_{\mathcal{R}}^2 - (\tilde{y} + M)^2}{\tilde{y} + M} \right| , \quad (44)$$

while \bar{p}_0 , related to the mass of the spectator system through

$$\bar{p}_0 = M - \sqrt{|\mathbf{p}_{min}|^2 + M_{\mathcal{R}}^2} , \quad (45)$$

can be simply parametrized in terms of the positive quantity B_0 according to

$$M_{\mathcal{R}} = M - m + B_0 . \quad (46)$$

The above discussion shows that the scaling analysis in terms of \tilde{y} involves two parameters: the constituent mass, m , and B_0 , playing the role of the constituent binding energy of many-body theory.

Fig.4 shows the quantities $W_1/\bar{\sigma}_1$ (upper panel) and $W_2/\bar{\sigma}_2$ (lower panel), obtained from DIS data taken at SLAC [16] and CERN [17,18] and rearranged in bins of constant $|\mathbf{q}|$ centered at 11, 19 and 27 GeV, plotted as a function of \tilde{y} . The structure functions W_1 have been obtained from the tabulated $F_2 = \nu W_2$ using the parametrization of $R = \sigma_L/\sigma_T$ of ref. [19], while the elementary cross sections have been evaluated from Eqs.(28)-(29) and (37)-(38), with $m = 300$ MeV and $B_0 = 200$ MeV. It clearly appears that in both cases scaling sets in at $|\mathbf{q}| > 10$ GeV. The second feature predicted by the IA analysis, i.e. that $W_1/\bar{\sigma}_1$ and $W_2/\bar{\sigma}_2$ scale to the *same* function $F(\tilde{y})$, is illustrated in fig.5.

It has to be emphasized that the occurrence of \tilde{y} scaling *does not* depend upon the values of either m or B_0 . In particular, it does not require that the constituent mass be negligibly small, nor that the struck constituent be on mass shell. Varying m and B_0 in the range 10 – 300 MeV does not appreciably affect the scaling behavior displayed in figs.4 and 5. However, it *does* affect the scaling function extracted from the data.

While increasing m at fixed B_0 leads to a shift of $F(\tilde{y})$ towards lower \tilde{y} for $\tilde{y} > -.5$ GeV, increasing B_0 at fixed constituent mass produces a shift in the opposite direction. As a result, the scaling function turns out to be only sensitive to the difference $m - B_0$, i.e. to the mass of the recoiling spectator system $M_{\mathcal{R}}$. This feature is illustrated in fig.Fig.6, showing that the scaling functions corresponding to $m = 110$ MeV, $B_0 = 10$ MeV and $m = 300$ MeV, $B_0 = 200$ MeV, yielding the same value of $M_{\mathcal{R}}$, lie on top of one another.

C. Comparison between \tilde{y} - and x -scaling analysis

DIS data are usually analyzed in terms of the two dimensionless structure functions $F_1 = MW_1$ and $F_2 = \nu W_2$. In the Bjorken limit $Q^2, \nu \rightarrow \infty$, with Q^2/ν finite and $\nu/|\mathbf{q}| \rightarrow 1$, both F_1 and F_2 exhibit scaling, i.e. they become functions of a single variable $x = Q^2/2M\nu$.

The first issue to be addressed to establish a connection between x - and \tilde{y} -scaling is the relation between the scaling variables. As pointed out in ref. [6], \tilde{y} is trivially related to another variable commonly used in the context of DIS, the Nachtmann variable ξ [7], through

$$-\frac{\tilde{y}}{M} = \xi = \frac{2x}{1 + \sqrt{1 + 4M^2x^2/Q^2}}, \quad (47)$$

where x is the Bjorken variable. From the above equation it follows that in the $Q^2 \rightarrow \infty$ limit \tilde{y} coincides with x up to a constant factor. Comparison between x and $-\tilde{y}/M$ at constant $|\mathbf{q}| = 20$ MeV shows that the difference is in fact less than 2 % over the whole $0 \leq x \leq 1$ range.

The correspondence between \tilde{y} and ξ makes it clear why \tilde{y} is better suited than y for the analysis of DIS. In addition, it has to be pointed out that the IA scheme provides a simple physical interpretation of Nachtmann's variable, whose definition was originally obtained in a totally different fashion [7].

As F_1 and F_2 are known to scale in x and the Bjorken variable is nearly proportional to \tilde{y} , they obviously scale in \tilde{y} as well. Figs. 7 and 8 show that F_1 and F_2 do indeed exhibit \tilde{y} -scaling at fixed $|\mathbf{q}|$, whereas W_2 does not. Note that the data plotted in Figs. 7 and 8 span a wide range of Q^2 , extending from 1.7 to 37.5 GeV².

It is very important to realize that, while \tilde{y} essentially coincides with $-Mx$, the scaling function $F(\tilde{y})$ cannot be identified with either F_1 or F_2 . The structure of $F(\tilde{y})$ is entirely dictated by the internal dynamics of the target, whereas both $F_1 = M\bar{\sigma}_1 F$ and $F_2 = \nu\bar{\sigma}_2 F$ contain part of the cross section describing the electron-constituent interaction. The shape of F_1 and F_2 is in fact strongly affected by the presence of the electromagnetic cross section. For example, at $\tilde{y} = 0$ gauge invariance requires F_2 to vanish, whereas F_1 must be proportional to the photoabsorption cross section. The \tilde{y} -scaling behavior displayed by F_1 and F_2 is a consequence of the fact that, besides the proton response F , $\bar{\sigma}_1$ and $\nu\bar{\sigma}_2$ also scale. This feature is illustrated in Fig.9, showing that $\bar{\sigma}_1$ and $\nu\bar{\sigma}_2$, plotted as a function of \tilde{y} , do not depend on $|\mathbf{q}|$ for $|\mathbf{q}| > 10$ GeV.

The different pictures emerging from x - and \tilde{y} -scaling analyses can only be reconciled

making the standard assumption of parton model that the constituent mass be negligibly small. As shown in fig. 10, as $m \rightarrow 0$

$$\bar{\sigma}_1 \rightarrow 1 \quad , \quad \bar{\sigma}_2 \rightarrow \frac{Q^2}{|\mathbf{q}|^2} \quad (48)$$

implying in turn that, in the Bjorken limit,

$$F_1 = MF(\tilde{y}) \quad , \quad F_2 = \nu \frac{Q^2}{|\mathbf{q}|^2} F(\tilde{y}) = 2xF_1 \quad , \quad (49)$$

and the standard picture of DIS is recovered. However, it has to be emphasized that, although in textbook derivations the requirement $m \sim 0$ is often introduced as a necessary condition for scaling in DIS, the present analysis shows that scaling occurs irrespective of the constituent mass.

V. IMPLICATIONS OF THE PROPOSED ANALYSIS

The differences between \tilde{y} -scaling analysis and the standard x -scaling analysis, based on the parton model, have several interesting implications for both the theoretical description of DIS and the interpretation of experimental data.

The fact that the data appear to be compatible with the naive description of the proton in terms of massive bound constituents suggests that past attempts to describe DIS within the constituent quark model (CQM) [20,21] may have to be reconsidered.

Within the CQM, the valence quark distributions at low resolution scale $Q_0^2 \sim \mu_0^2 \sim (M/3)^2$, $u_v(x, Q_0^2)$ and $d_v(x, Q_0^2)$, are obtained from quark momentum distributions and used as a starting point for QCD evolution to the Q^2 scale relevant to DIS data. As an illustrative example of this procedure, fig. 11 shows the valence quarks contribution to the proton structure function F_2 , evaluated in ref. [20] using a harmonic oscillator quark momentum distribution, before (dashed line) and after (dot-dash line) QCD evolution until $Q^2 = 15 \text{ GeV}^2$. The authors of ref. [20] chose a constituent mass $m = M/3$ and adjusted the harmonic oscillator frequency in such a way as to reproduce the experimental value of the proton rms charge radius.

The approach proposed in this paper provides a consistent alternative framework to calculate the proton structure functions from CQM momentum distributions. For any given momentum distribution $n(\mathbf{p})$, $F_2 = \nu W_2$ can in fact be obtained from Eq.(31) using $P(p) = n(\mathbf{p})\delta(p_0 - \bar{p}_0)$, \bar{p}_0 being defined in terms of the parameter B_0 through Eqs.(45) and (46).

The structure function F_2 obtained using the same constituent mass and momentum distribution as in ref. [20] and $B_0 = 200$ MeV is shown by the solid line in fig. 11. Note that in the CQM calculation of the distributions $u_v(x, Q_0^2)$ and $d_v(x, Q_0^2)$, the constituent quarks are assumed to be on mass shell. As a consequence, $M_{\mathcal{R}} = M - m$, implying in turn $B_0 = 0$.

Inclusion of binding, described by $B_0 \neq 0$, leads to the appearance of strength in the region $\tilde{y} > -.10$ GeV, where the structure function of ref. [20] vanishes. The mechanism responsible for this feature can be readily understood with the help of fig. 12, showing the domains of the $(M_{\mathcal{R}}^2, |\mathbf{p}|)$ plane relevant to the calculation of the proton structure functions at $|\mathbf{q}| = 10$ GeV and $\tilde{y} = 0, -200$ MeV and -350 MeV using Eq.(31).

In the CQM, as the quark energy distribution is a δ -function requiring $B_0 = 0$, the integration is carried out along the horizontal line $M_{\mathcal{R}}^2 = (M - m)^2$, corresponding to the lower limit of the kinematically allowed domains. The maximum of the response is located to $\tilde{y} = -m$, because in this case the lower limit of the momentum integration is $|\mathbf{p}_{min}| = 0$. Larger \tilde{y} corresponds to larger $|\mathbf{p}_{min}|$, leading in turn to a smaller response, as the quark momentum distribution is a rapidly decreasing function of $|\mathbf{p}|$. For example, at $\tilde{y} = -.10$ GeV $n(|\mathbf{p}_{min}|)/n(|\mathbf{p}| = 0) \sim 1\%$. Setting $B_0 \neq 0$, which amounts to carrying out the integration along the horizontal line $M_{\mathcal{R}}^2 = (M - m + B_0)^2$, leads to a decrease of $|\mathbf{p}_{min}|$ at $\tilde{y} > -m$, i.e. to an increase of the response. At $\tilde{y} = -.1$ GeV, one finds that $B_0 = 0$ and 200 MeV correspond to $|\mathbf{p}_{min}| = .20$ and $.01$ GeV, respectively.

The fact that scaling in \tilde{y} occurs irrespective of the values of m and B_0 , the resulting scaling function being roughly determined by the difference $m - B_0$, i.e. by the mass of the spectator system $M_{\mathcal{R}}$, poses a serious problem for the extraction of $F(\tilde{y})$ from the data and its interpretation. Even under the standard parton model assumption of negligibly small mass, allowing the constituent to be off mass shell leads to a shift of $F(\tilde{y})$ towards larger \tilde{y} .

In ref. [6] it has been pointed out that if binding effects are large, i.e. if the energy distribution of the constituents extends into the region of large $M_{\mathcal{R}}$, which dominates the response at $\tilde{y} \sim 0$ (see fig. 12), they may result in part of the response being pushed into the timelike region $\nu > |\mathbf{q}|$, inaccessible to electron scattering. The occurrence of strength located in the timelike region is a well known feature of the response of interacting many-body systems, simply reflecting the fact that there is no *a priori* reason preventing the target from being left in a final state with energy $E_n > E_0 + |\mathbf{q}|$, where E_0 is the energy of the initial state. On the other hand, in the case of noninteracting systems the inequality $\nu < |\mathbf{q}|$ is always satisfied and the response can be shown to vanish identically for $\tilde{y} > 0$. This issue has been recently investigated in ref. [22], whose authors have shown that $\sim 10\%$ of the strength associated with the response of a confined relativistic particle is indeed located in the region of positive \tilde{y} .

Obviously, the presence of strength in the timelike region would make the experimental verification of some rules involving the proton response, e.g. the Gross-Llewellyn Smith sum rule [23], impossible. This problem has long been recognized in the analysis of electron-nucleus scattering data. For example, integration of the measured charge response of iron at momentum transfer $|\mathbf{q}| = 570$ MeV yields only $\sim 90\%$ of the nuclear charge Z [24].

VI. CONCLUSIONS

The results described in this paper show that the scaling analysis of scattering processes off many-body systems, successfully employed to describe neutron-liquid helium and electron-nucleus scattering, can be extended to the case of DIS of electrons by protons.

The data exhibit a remarkable scaling behavior in the natural variable of many-body theory, whose definition and interpretation naturally emerge from the analysis of the scattering process in the target rest frame. The onset of \tilde{y} -scaling follows from the assumptions underlying the IA picture. No further assumptions on the mass and binding energy of proton constituents are required.

While in the Bjorken limit \tilde{y} essentially coincides with x , up to a constant factor, the scaling function $F(\tilde{y})$ cannot be trivially related to the structure functions $F_1(x)$ and $F_2(x)$, whose behavior is dictated by both the internal proton dynamics and the electromagnetic electron-constituent interaction. The correspondence between $F(\tilde{y})$ and $F_1(x)$ and $F_2(x)$ can only be established in the limit of vanishing constituent mass.

The function $F(\tilde{y})$, which can be identified with the target response in the scaling limit, turns out to be significantly affected by binding effects, the position of its peak being mainly dictated by the mass of the spectator system $M_{\mathcal{R}}$.

The structure function F_2 calculated from Eq.(31) appreciably differs from the prediction of the CQM at low resolution scale. Comparison between the solid and dashed curves of fig. 12 shows that the treatment of binding and mass according to the approach discussed in this paper produces an effect qualitatively similar to that of QCD evolution, shifting strength towards larger \tilde{y} . The results displayed in fig. 12 suggest that the role of QCD evolution should be reassessed, using the structure function represented by the solid line as a starting point.

Binding effects, resulting in a shift of $F(\tilde{y})$ towards larger values of \tilde{y} , can also push a fraction of the strength into the region of positive \tilde{y} , inaccessible to DIS experiments. The proposed analysis, being carried out at fixed $|\mathbf{q}|$, appears to be best suited to address this feature, as moving along lines of constant $|\mathbf{q}|$ one intersects the photon line $\nu = |\mathbf{q}|$ and enters the timelike region, while moving along lines of constant $Q^2 > 0$, as generally done in the analysis of DIS, the photon line is only asymptotically approached [6].

Finally, it has to be pointed out that the observation of scaling *does not* necessarily imply the validity of the assumptions underlying the IA picture, i.e. dominance of incoherent scattering and absence of FSI. It has been shown that, both in neutron-liquid helium scattering [25] and in electron-nucleus scattering [26], as long as the cross section describing the interactions between target constituents does not depend upon $|\mathbf{q}|$, FSI *do not* prevent the occurrence of scaling. However, in presence of FSI the scaling function extracted from the data *can not* be related to the initial momentum and energy distribution of target

constituents.

The results of ref. [27] indicate that sizable FSI effects in the response of a scalar relativistic particle confined by a linear potential persist in the kinematical regime of large $|\mathbf{q}|$, in which \tilde{y} -scaling is clearly observed. The role of FSI in DIS and their impact on the interpretation of the measured proton structure functions have been recently discussed in refs. [28,29], whose authors conclude that the DIS cross section is indeed affected by final state rescatterings, and can not be simply related to the parton distributions in the initial state.

ACKNOWLEDGMENTS

The author is deeply indebted to Vijay R. Pandharipande and Ingo Sick for many illuminating discussions on different issues related to the subject of this paper. The hospitality of the Theory Group at the Thomas Jefferson National Accelerator Facility and the partial support of the U.S. Department of Energy during the completion of this work are also gratefully acknowledged.

APPENDIX A: TARGET ELECTROMAGNETIC TENSOR WITHIN IA

The general expression of the target electromagnetic tensor

$$W^{\mu\nu} = \sum_n \int d^3p_n \langle 0 | J^\mu | n \rangle \langle n | J^\nu | 0 \rangle \delta^{(4)}(P_0 + q - P_n) \quad (\text{A1})$$

drastically simplifies under the assumptions underlying the IA scheme, which lead to rewrite the target current and final state as (the index i labels the struck constituent)

$$J^\mu \rightarrow \sum_i j_i^\mu \quad (\text{A2})$$

and

$$|n\rangle \rightarrow |\mathbf{p}', \mathcal{R}\rangle = |i(\mathbf{p}')\rangle \otimes |\mathcal{R}(\mathbf{p}_R)\rangle . \quad (\text{A3})$$

In the above equations j_i^μ is the current associated to a target constituent, whereas the states $|i(\mathbf{p}')\rangle$ and $|\mathcal{R}(\mathbf{p}_R)\rangle$ describe the struck constituent and the spectator system, respectively (see the discussion following eq.(9)). The structure of the IA final state can be exploited to rewrite the sum appearing in Eq.(A1) replacing

$$\sum_n |n\rangle\langle n| \rightarrow \int d^3p' |\mathbf{p}'\rangle\langle\mathbf{p}'| \sum_{\mathcal{R}} |\mathcal{R}\rangle\langle\mathcal{R}| . \quad (\text{A4})$$

Substitution of Eqs.(A2)-(A4) into Eq.(A1) and insertion of complete sets of free particle states, satisfying

$$\int d^3p |\mathbf{p}\rangle\langle\mathbf{p}| = I , \quad (\text{A5})$$

yields the expression

$$W^{\mu\nu} = \sum_i \sum_{\mathcal{R}} \int d^3p d^3p' |\langle 0|\mathbf{p}, \mathcal{R}\rangle|^2 \langle\mathbf{p}|j_i^\mu|\mathbf{p}'\rangle\langle\mathbf{p}'|j_i^\nu|\mathbf{p}\rangle \times \delta^{(3)}(\mathbf{q} + \mathbf{p} - \mathbf{p}')\delta(\nu + E_0 - E_{\mathcal{R}} - E_{\mathbf{p}'}) , \quad (\text{A6})$$

that can be further rewritten in a more compact form in terms of the constituent momentum end energy distribution $P(p)$, defined by Eq.(12). As a result we obtain

$$W^{\mu\nu} = \sum_i \int d^4p P(p) \int d^3p' \langle\mathbf{p}|j_i^\mu|\mathbf{p}'\rangle\langle\mathbf{p}'|j_i^\nu|\mathbf{p}\rangle \delta^{(3)}(\mathbf{q} + \mathbf{p} - \mathbf{p}')\delta(\nu + p_0 - E_{\mathbf{p}'}) . \quad (\text{A7})$$

Finally, we can substitute in the above equation the definition of the electromagnetic tensor corresponding to scattering at four-momentum transfer $q \equiv (\nu, \mathbf{q})$ off a *free* constituent carrying momentum \mathbf{p} :

$$w_i^{\mu\nu} = \int d^3p' \langle\mathbf{p}|j_i^\mu|\mathbf{p}'\rangle\langle\mathbf{p}'|j_i^\nu|\mathbf{p}\rangle \delta^{(3)}(\mathbf{q} + \mathbf{p} - \mathbf{p}')\delta(\nu + E_{\mathbf{p}} - E_{\mathbf{p}'}) . \quad (\text{A8})$$

Comparison of Eqs.(A7) and (A8) shows that $W^{\mu\nu}$ can be rewritten in the form

$$W^{\mu\nu} = \sum_i \int d^4p P(p) w_i^{\mu\nu}(\tilde{p}, \tilde{q}) , \quad (\text{A9})$$

where $\tilde{p} \equiv (E_{\mathbf{p}}, \mathbf{p})$ and $\tilde{q} \equiv (\tilde{\nu}, \mathbf{q})$, with $\tilde{\nu} = E_{\mathbf{p}+\mathbf{q}} - E_{\mathbf{p}} = \nu + p_0 - E_{\mathbf{p}}$.

APPENDIX B: RESTORATION OF GAUGE INVARIANCE

The definition of the tensor $W^{\mu\nu}$ given by Eq.(A9) obviously leads to breaking gauge invariance, as

$$q_\mu w_i^{\mu\nu}(\tilde{p}, \tilde{q}) \neq 0 \quad (\text{B1})$$

by construction.

The prescription proposed in ref. [12] to circumvent this problem amounts to using IA only for the transverse and time components of the current j_i^μ . Denoting by $\tilde{w}_{\mu\nu}$ the electromagnetic tensor of ref. [12] and choosing the z -axis along the direction of \mathbf{q} we can then write

$$\tilde{w}_i^{\mu\nu}(p, q) = w_i^{\mu\nu}(\tilde{p}, \tilde{q}) \quad , \quad \mu, \nu \neq 3 \quad . \quad (\text{B2})$$

The longitudinal current j_i^3 is defined in terms of the time component j_i^0 in such a way as to satisfy the continuity equation. As a result, the corresponding elements of the tensor $\tilde{w}_i^{\mu\nu}$ read

$$\tilde{w}_i^{\mu 3}(p, q) = \left(\frac{\nu}{|\mathbf{q}|} \right) w_i^{\mu 0}(\tilde{p}, \tilde{q}) \quad (\text{B3})$$

and

$$\tilde{w}_i^{33}(p, q) = \left(\frac{\nu}{|\mathbf{q}|} \right)^2 w_i^{00}(\tilde{p}, \tilde{q}) \quad . \quad (\text{B4})$$

The above procedure to reconcile the IA scheme with gauge invariance is manifestly non unique. However, it has to be emphasized that, since according to ref. [12] the current satisfies the relation $\tilde{j}^3 = (\nu/|\mathbf{q}|)j^0$, while the IA current satisfies $j^3 = (\tilde{\nu}/|\mathbf{q}|)j^0$, the difference

$$\tilde{j}^3 - j^3 = \frac{\nu - \tilde{\nu}}{|\mathbf{q}|} = \frac{E_{\mathbf{p}} - p_0}{|\mathbf{q}|} \quad , \quad (\text{B5})$$

providing a measure of the violation of gauge invariance, becomes vanishingly small in the $|\mathbf{q}| \rightarrow \infty$ limit.

REFERENCES

- [1] G.B. West, Phys. Rep. **18**, 263 (1975)
- [2] T.R. Sosnick, W.M. Snow, R.N. Silver and P.E. Sokol, Phys. Rev. B **43**, 216 (1991).
- [3] D.B. Day, J.S. Mc Carthy, T.W. Donnelly and I. Sick, Ann. Rev. Nucl. Part. Sci. **40**, 357 (1990).
- [4] J.I. Friedman and H.W. Kendall, Ann. Rev. Nucl. Sci. **22**, 203 (1972).
- [5] G.B. West, in *Momentum distributions*, edited by R.N. Silver and P.E. Sokol (Plenum, New York, 1989) pp. 95-110.
- [6] O. Benhar, I. Sick and V.R. Pandharipande, Phys. Lett. **B 489**, 131 (2000).
- [7] O. Nachtman, Nucl. Phys. **B 63**, 237 (1973).
- [8] O. Benhar, A. Fabrocini and S. Fantoni, Phys. Rev. Lett. **87**, 052501 (2001).
- [9] R.T. Arzula *et al*, Phys. Rev. B **56**, 14620 (1997).
- [10] H. R. Glyde, Phys. Rev. B **50**, 6726 (1994).
- [11] F.E. Close *An Introduction to Quarks and Partons* (Academic Press, London, 1979).
- [12] T. de Forest, Jr., Nucl. Phys. **A392**, 232 (1983).
- [13] Z. Batiz and F. Gross, Phys. Rev. C **58**, 2963(1998).
- [14] J. Arrington *et al*, Phys. Rev. C **64**, 014602 (2001).
- [15] C. Ciofi degli Atti, E. Pace and G. Salmè, Phys. Rev. C **43**, 1155 (1991).
- [16] L. W. Whitlow *et al*, Phys. Lett. **B282**, 475 (1992).
- [17] M. Arneodo, *et al*, Nucl. Phys. **B483**, 3 (1997).
- [18] A.C. Benvenuti *et al*, Phys. Lett. **B223**, 485 (1989).

- [19] L. W. Whitlow, S. Rock, A. Bodek, S. Dasu and E.M. Riordan, Phys. Lett. **B250**, 193 (1990).
- [20] M.Traini, L. Conci and U. Moschella, Nucl. Phys. **A544**, 731 (1992).
- [21] F.M. Steffens and A.W. Thomas, Nucl. Phys. **A568**, 798 (1994).
- [22] M.W. Paris and V.R. Pandharipande, Phys. Lett. **B514**, 361 (2001).
- [23] I. Hinchliffe and A. Kwiatowski, Ann. Rev. Nucl. Part. Sci. **46**, 609 (1996).
- [24] J. Jourdan, Nucl. Phys. A **603**, 117 (1996).
- [25] J.J. Weinstein and J.W. Negele, Phys. Rev. Lett. **49**, 1016 (1982).
- [26] O. Benhar, Phys. Rev. Lett. **83**, 3130 (1999).
- [27] M.W. Paris and V.R. Pandharipande, Phys. Rev. C **65**, 035203 (2002).
- [28] S.J. Brodsky, P. Hoyer, N. Marchal, S. Peigné and F. Sannino, hep-ph/0104291.
- [29] S. Peigné and F. Sannino, hep-ph/0112080.

FIGURES

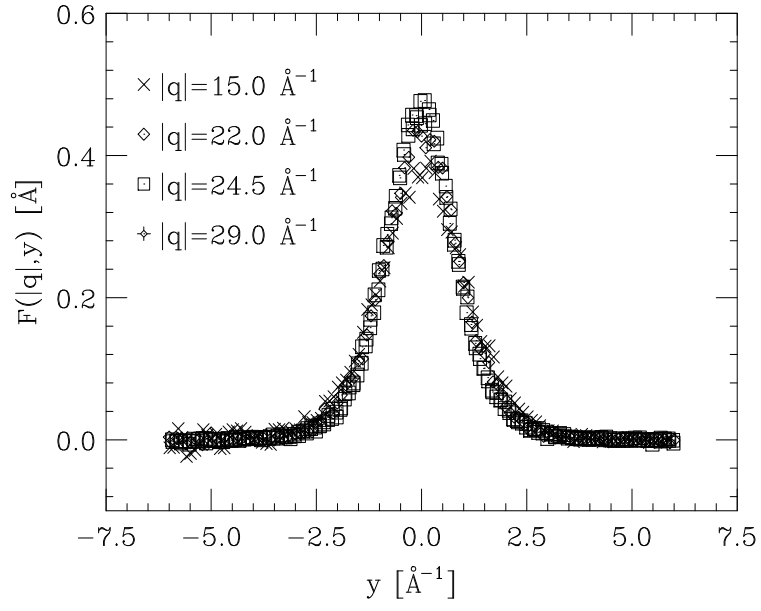


FIG. 1. Scaling functions $F(y)$, defined as in Eq.(19), measured by neutron scattering off superfluid ^4He at $T=1.6 \text{ }^\circ\text{K}$ [9]. The data sets are labelled according to the magnitude of the momentum transfer $|\mathbf{q}|$.

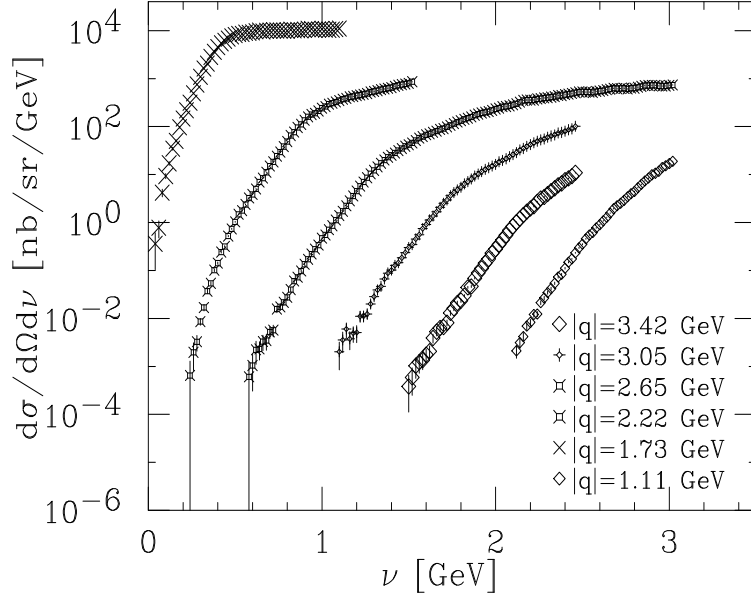


FIG. 2. Cross sections for scattering of 4 GeV electrons off Iron, plotted as a function of the electron energy loss. The data sets are labelled according to the momentum transfer at the quasielastic peak [14].

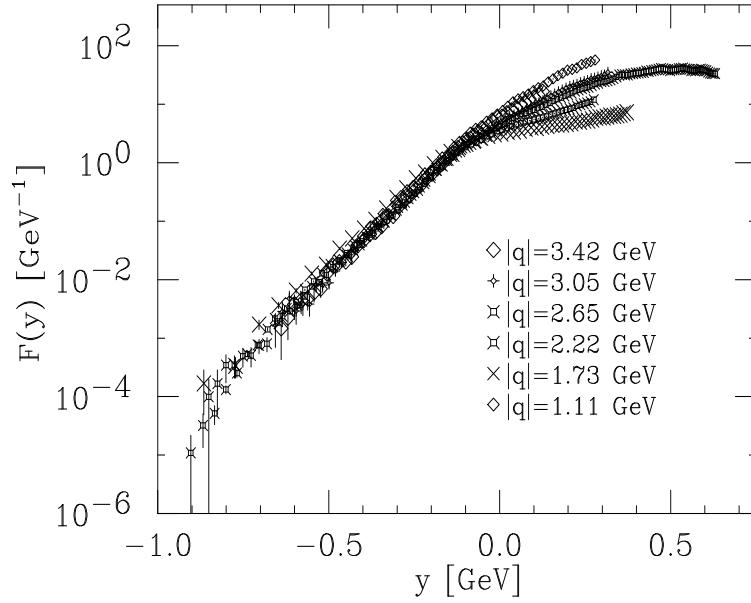


FIG. 3. Scaling functions obtained from the definitions of Eqs.(35) and (36) using the cross sections shown in fig.2 [14].

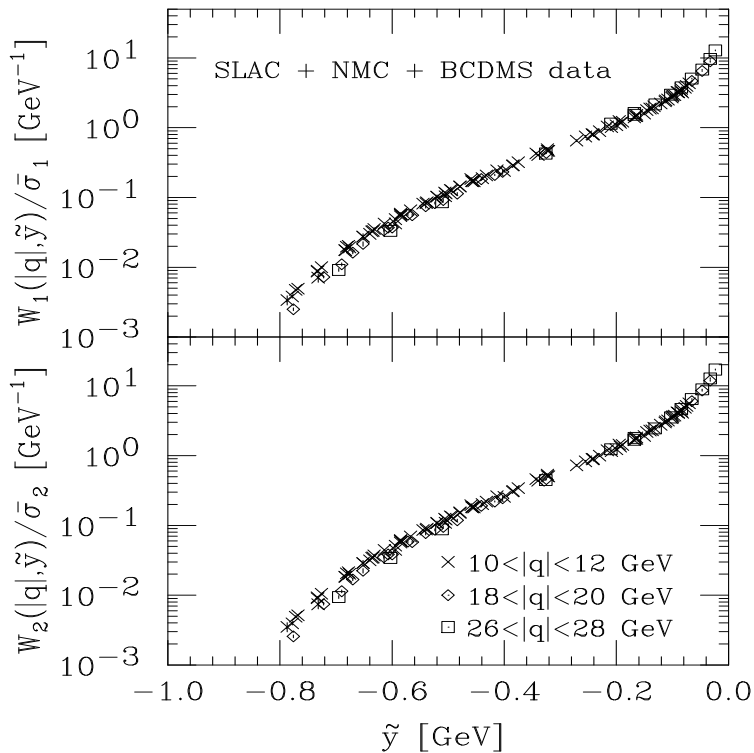


FIG. 4. Scaling functions obtained from $W_1/\bar{\sigma}_1$ (upper panel) and $W_2/\bar{\sigma}_2$ (lower panel). The experimental structure functions are taken from refs. [16–18] and labelled according to the values of $|\mathbf{q}|$, whereas the elementary cross sections have been evaluated using Eqs.(28)-(29) and (37)-(38), with $m = 300$ MeV and $B_0 = 200$ MeV.

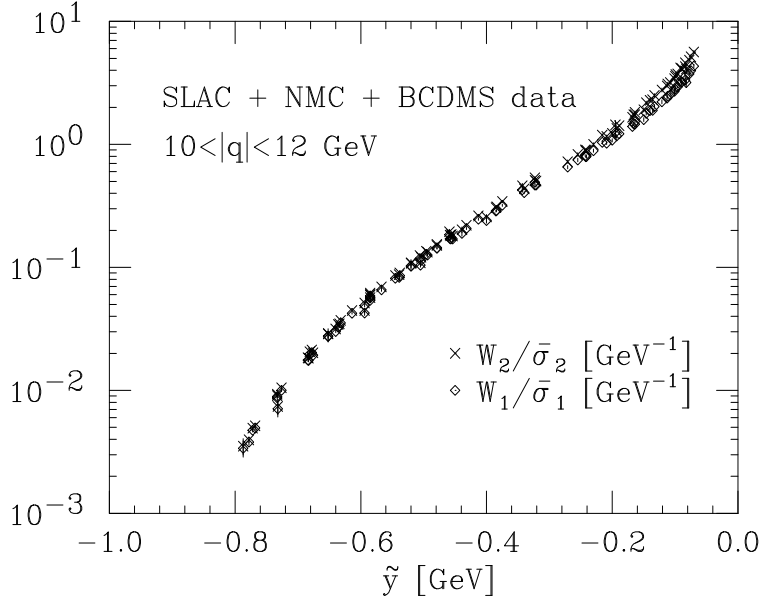


FIG. 5. Comparison between $W_1/\bar{\sigma}_1$ (diamonds) and $W_2/\bar{\sigma}_2$ (crosses) of fig. 4 at $10 \leq |\mathbf{q}| \leq 12$ GeV.

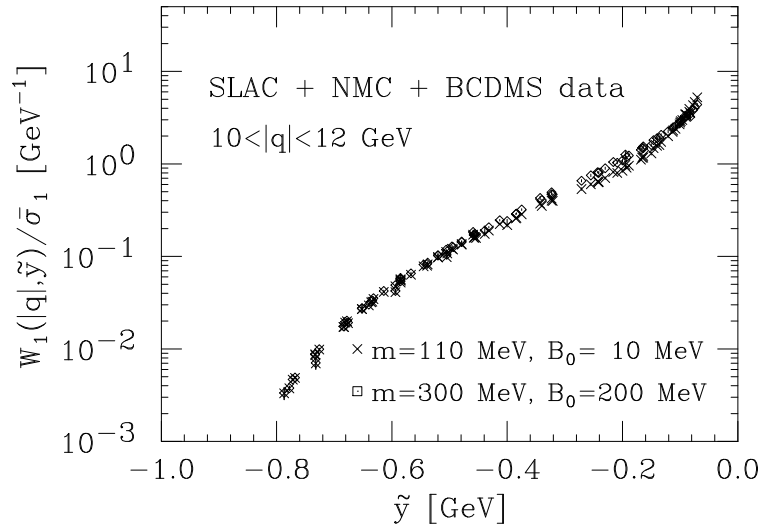


FIG. 6. \tilde{y} -scaling function obtained from the structure functions of refs. [16–18] corresponding to $10 \leq |\mathbf{q}| \leq 12$ GeV. Crosses and diamonds represent the results obtained using $m = 110$ MeV, $B_0 = 10$ MeV and $m = 300$ MeV, $B_0 = 200$ MeV, respectively.

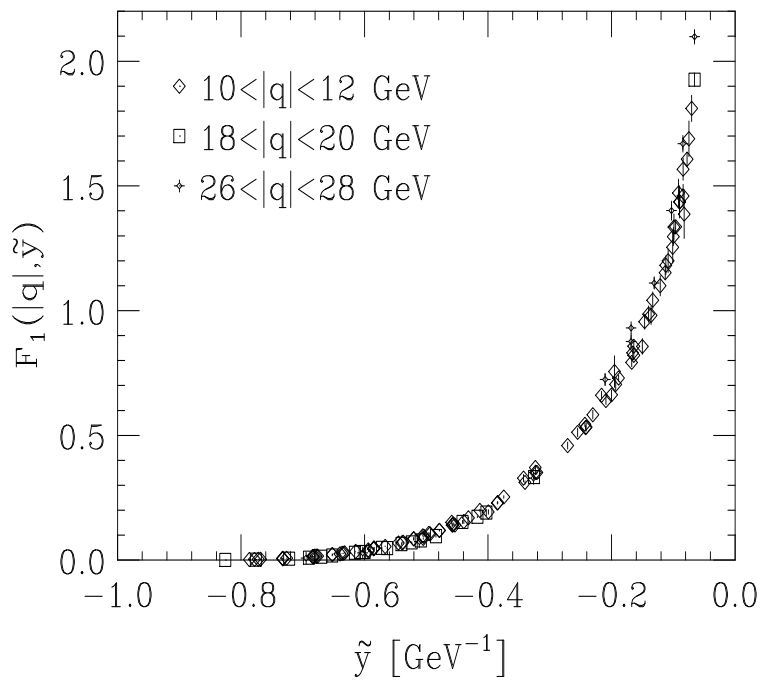


FIG. 7. \tilde{y} -dependence of the structure function $F_1 = MW_1$ obtained from the data of refs. [16–18]. The data sets are labelled according to the values of $|\mathbf{q}|$.

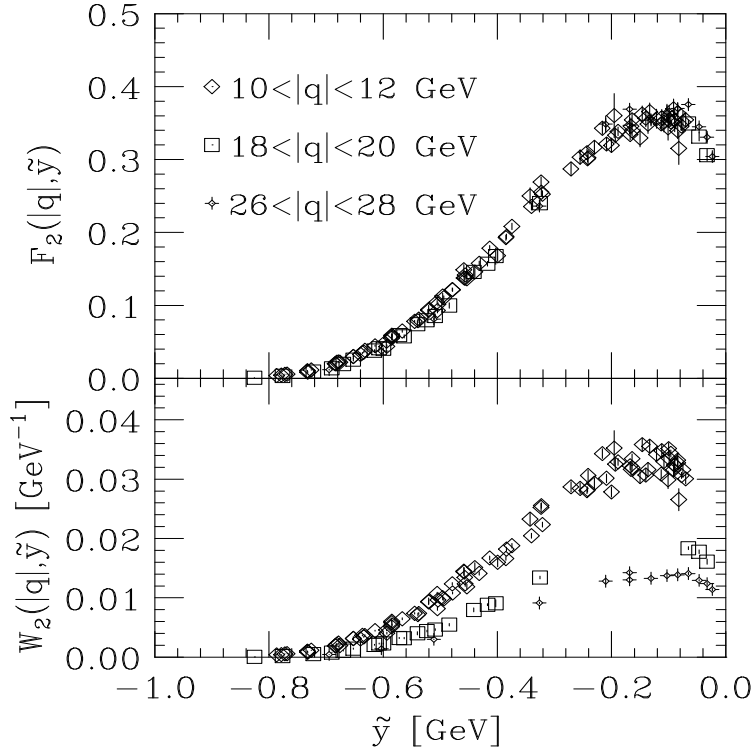


FIG. 8. \tilde{y} -dependence of W_2 (lower panel) and $F_2 = \nu W_2$ (upper panel) obtained from the data of refs. [16–18]. The data sets are labelled according to the values of $|q|$.

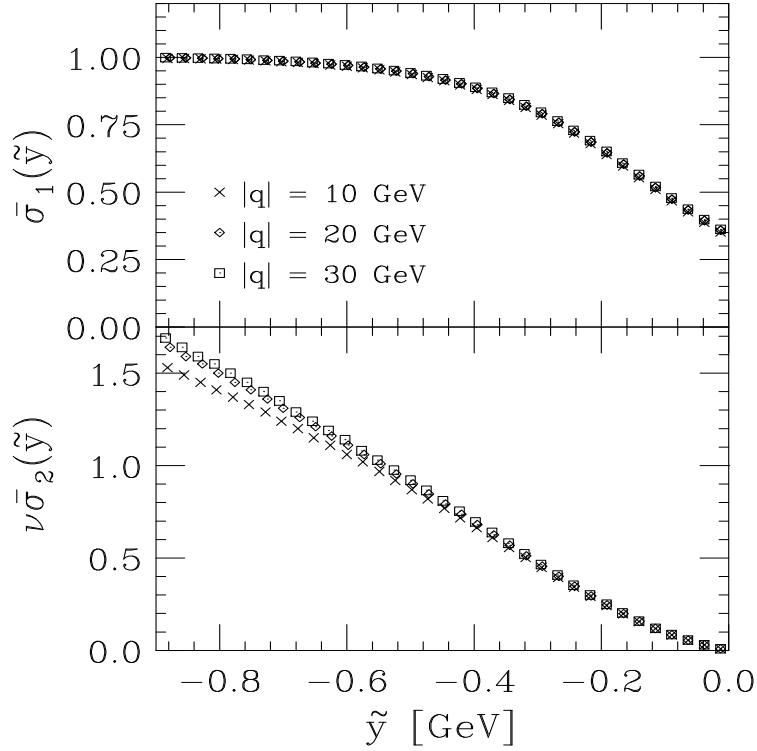


FIG. 9. Dependence of $\bar{\sigma}_1$ (upper panel) and $\nu\bar{\sigma}_2$ (lower panel), given by Eqs.(28)-(29) and (37)-(38), upon the momentum transfer $|\mathbf{q}|$. Crosses, diamonds and squares correspond to $|\mathbf{q}| = 10, 20$ and 30 GeV, respectively. All calculations have been carried using $m = 300$ MeV and $B_0 = 200$ MeV.

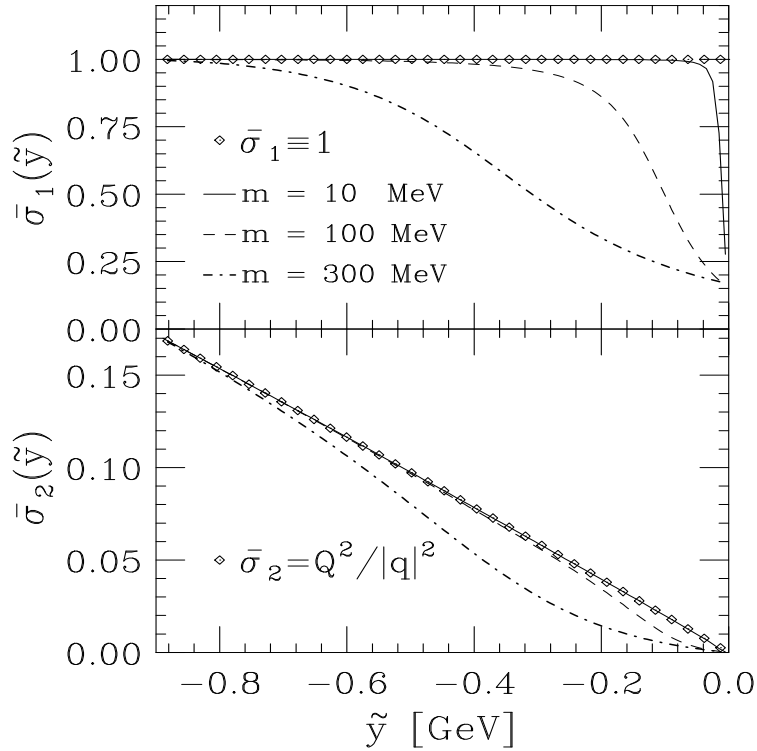


FIG. 10. Dependence of the elementary electron-constituent cross sections $\bar{\sigma}_1$ (upper panel) and $\bar{\sigma}_2$ (lower panel), given by Eqs.(28)-(29) and (37)-(38), upon the constituent mass. The solid, dashed and dot-dash lines correspond to $m = 10, 100$ and 300 MeV, respectively, whereas the diamonds show the $m \rightarrow 0$ limit. All calculations have been carried at $|\mathbf{q}| = 10$ GeV and using $B_0 = 0$.

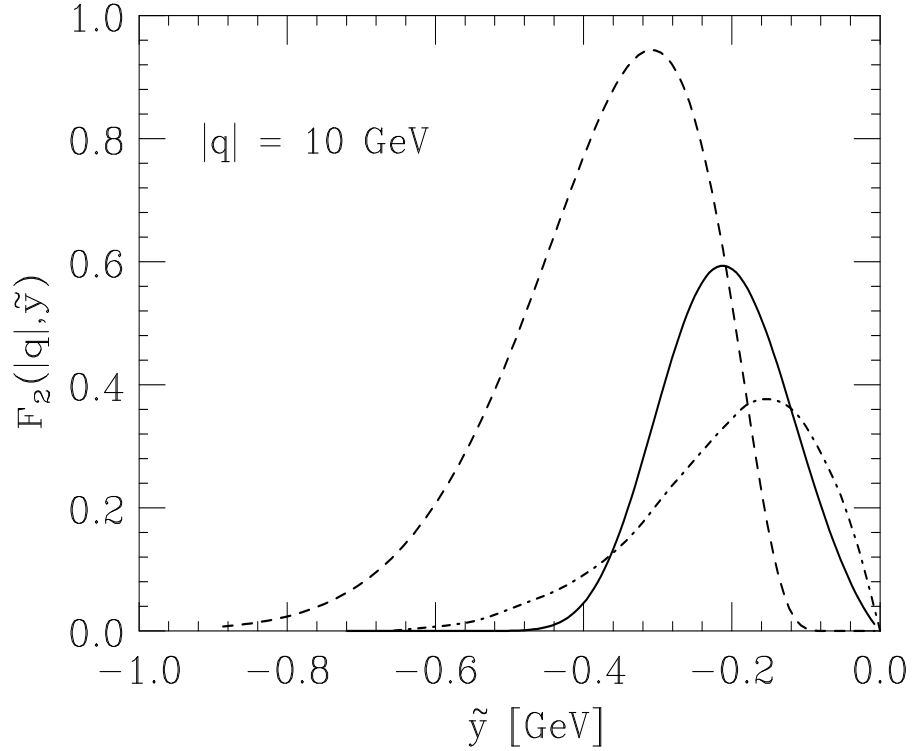


FIG. 11. Valence quarks contribution to the proton F_2 , plotted as a function of \tilde{y} at constant $|\mathbf{q}| = 10$ GeV. The dashed and dash-dot lines show the results of the constituent quark model of ref. [20] before and after QCD evolution until $Q^2 = 15$ GeV², respectively. The solid line shows F_2 obtained within the approach described in this paper, using the same quark mass and momentum distribution as in ref. [20] and $B_0 = 200$ MeV.

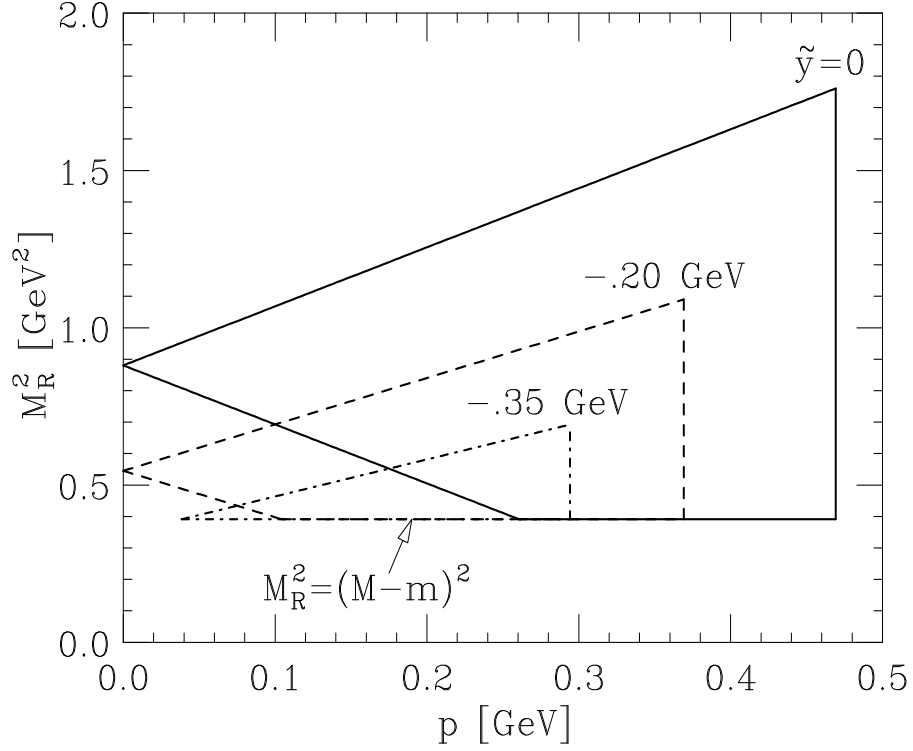


FIG. 12. Domains of the $(M_R^2, |\mathbf{p}|)$ plane relevant to the calculation of the proton structure functions at $|\mathbf{q}| = 10$ GeV and $\tilde{y} = 0$ (solid line), -200 MeV (dashed line) and -350 MeV (dot-dash line) from Eq.(31). The results have been obtained using $m = M/3$.